Optical transition energies of isolated molecular monomers and weakly interacting two-dimensional aggregates

Roman Forker,[1,*] Thomas Dienel,[2] Andreas Krause,[3] Marco Gruenewald,[1] Matthias Meissner,[1] Tino Kirchhuebel,[1] Oliver Gröning,[2] and Torsten Fritz[1,4]

[1]*Institute of Solid State Physics, Friedrich Schiller University Jena, Helmholtzweg 5, D-07743 Jena, Germany*

[2]*Nanotech@surfaces Laboratory, EMPA–Swiss Federal Laboratories for Materials Science and Technology, Ueberlandstrasse 129, CH-8600 Duebendorf, Switzerland*

[3]*NaMLab gGmbH, Noethnitzer Str. 64, D-01187 Dresden, Germany*

[4]*Osaka University, Graduate School of Science and Institute for Academic Initiatives, Department of Chemistry, 1-1 Machikaneyama, Toyonaka 560-0043, Osaka, Japan*

(Received 12 November 2015; revised manuscript received 10 March 2016; published 19 April 2016)

The optical excitation energies of organic dye molecules are often said to depend sensitively on the polarizability of the utilized substrate. To this end, we employ differential reflectance spectroscopy (DRS) to analyze the $S_0 \rightarrow S_1$ fundamental transition energies observed for 3,4,9,10-perylene tetracarboxylic dianhydride (PTCDA) as a function of coverage on various surfaces, such as sp^2-bonded insulating layers [graphene and hexagonal boron nitride (h-BN)], and noble metals pre-covered by a molecular wetting layer which prevents hybridization of the second-layer molecules with the metal states. We elucidate the optical absorbance behavior of PTCDA layers grown on h-BN/Rh(111) and on h-BN/Pt(111) and characterize their structures by means of scanning tunneling microscopy. Surprisingly, although the dielectric properties of the employed substrates differ substantially, only two main transition energies are observed: (i) $PTCDA_{HE}$ essentially mimics the behavior of isolated monomers on surfaces (particularly at submonolayer coverage), while (ii) $PTCDA_{LE}$, red-shifted by ≈ 70 meV (≈ 560 cm^{-1}), is attributed to two-dimensional densely packed aggregates. This red-shift is in remarkable accordance with previous investigations for PTCDA on NaCl(100) and, therefore, likely arises from the same physical effects, namely the formation of two-dimensional excitonic bands and the polarizability of neighboring molecules within the monolayer. In distinction from earlier studies, we conclude that the polarizabilities of the employed substrates do not constitute the dominant contribution to the molecular $S_0 \rightarrow S_1$ transition energies observed here.

DOI: 10.1103/PhysRevB.93.165426

I. INTRODUCTION

Typical organic optoelectronic devices often comprise stacked thin films of different materials designed to meet the demands of organic light-emitting diodes [1] (OLEDs) and organic solar cells [2] (OSCs), amongst others. Various strategies to enhance the performance of their components are being pursued: On the one hand, synthetic chemistry provides the toolbox for the tunability of optical and electronic properties of the molecular species [3]. On the other hand, these properties are also known to depend sensitively on the physical structure, i.e., the specific packing motif, bearing in mind that polymorphism is frequently encountered in organic bulk crystals and thin film structures [4]. For example, the α and β phases of zinc(II)-phthalocyanine were reported to exhibit clearly distinct optical absorbance spectra [5], and also their electrical conductivity is markedly different [6]. Furthermore, the physical properties associated with organic crystal structures are usually highly anisotropic [7–10]. This circumstance can be utilized, for instance, by adjusting molecular alignments to optimally absorb photons in OSCs [11] or to enable lasing operation of multilayer nanofibers [12]. Exploring and, consequently, exploiting these structure–property relations are thus necessary steps to achieve economically worthwhile device efficiencies.

Here, we investigate the optical properties focusing on the $S_0 \rightarrow S_1$ transition of submonolayers and monolayers (ML) of 3,4,9,10-perylene tetracarboxylic dianhydride (PTCDA, $C_{24}H_8O_6$, CAS registry No. 128-69-8). For PTCDA two monoclinic crystal structures (α and β phase) have been reported [13–16]. These structures are quite comparable, both exhibiting planar molecules which are almost parallel to the (102)-oriented crystal planes forming similar two-dimensional (2D) herringbone patterns. The bulk crystal structures are describable as stacked (102) planes; the molecules of adjacent planes are assembled face-to-face with small lateral offsets. By means of density functional theory (DFT) calculations [17] it has been shown in particular that the excited state wave functions in α-PTCDA crystals stretch out over roughly four molecules in the stacking direction, while to a much smaller extent they are also delocalized within the (102) planes, in consistence with earlier theoretical [18,19] and experimental [20,21] reports. Accordingly, PTCDA—as a prototype molecule with particularly anisotropic crystal structures—is often dubbed "quasi-one-dimensional material" [18–21].

In this contribution we employ *in situ* differential reflectance spectroscopy [DRS, cf. Eq. (1)] to assess the optical absorption behavior of PTCDA films adsorbed on sp^2-bonded layers, such as graphene on silicon carbide and metals covered by a hexagonal boron nitride (h-BN) or by a passivating molecular monolayer. For this purpose, measurements of PTCDA on h-BN/Rh(111) and h-BN/Pt(111) are compared to previous studies on various other substrates [22–25]. Surprisingly, only

*roman.forker@uni-jena.de

two distinct sets of $S_0 \rightarrow S_1$ transition energies (hereafter called $PTCDA_{HE}$ and $PTCDA_{LE}$ for high and low energy, respectively) are observed, although the dielectric properties of the substrates vary considerably. The energetic difference between $PTCDA_{HE}$ and $PTCDA_{LE}$ amounts to approximately 70 meV, which is almost exactly the same difference between herringbone domains and a dilute phase of PTCDA on NaCl(100) reported earlier [26]. However, in distinction from Ref. [26] we conclude that the spectral positions observed are only moderately influenced by substrate polarizabilities.

II. EXPERIMENTAL DETAILS

The Pt(111) and Rh(111) single crystals were cleaned by repeated cycles of Ar^+ sputtering (750 eV, grazing incidence) and annealing (1100 K), followed by short-time flashing to 1450 K in the case of Pt(111). On top of these substrates hexagonal boron nitride (h-BN) was grown by thermal dehydrogenation of borazine on the hot metal surfaces (1100 K) [27–30]. This process is self-limiting once the first h-BN monolayer fully covers the metal surfaces. To promote a uniform layer morphology the samples were subsequently annealed at 1000 K for 15 min. The surface corrugation of the h-BN layer is rather pronounced on Rh(111), with 0.7-Å-deep depressions dubbed holes or pores, surrounded by so-called ligaments or wires [31]. Contrary to that, the h-BN layer is rather flat on Pt(111) [32].

PTCDA raw material was purchased from Sigma-Aldrich (nominal purity 97%) and further purified by repeated temperature gradient sublimation cycles as described in Ref. [16]. After transfer to the deposition chambers the purified powder was degassed for several hours prior to any experiment. PTCDA films were then deposited from effusion cells.

Scanning tunneling microscopy (STM) experiments were performed in an ultrahigh vacuum (UHV) apparatus (base pressure $\approx 10^{-11}$ mbar) at EMPA equipped with a commercial low-temperature STM operated at ≈ 5 K (Omicron). A PtIr tip was cut and used without further treatment.

Optical spectroscopy experiments were performed at FSU Jena during film growth under UHV conditions (base pressure $< 3 \times 10^{-10}$ mbar) employing *in situ* DRS. The measured signal is defined as

$$\mathrm{DRS}(E,d) := \frac{R(E,d) - R(E,0)}{R(E,0)}. \qquad (1)$$

$R(E,0)$ denotes the reflectance of the bare substrate at photon energy E, while $R(E,d)$ is the reflectance recorded during film growth at a nominal adsorbate thickness d. The setup has been detailed previously [21,33]. For the spectral analysis the following substrates are used: h-BN/Rh(111) (this work), h-BN/Pt(111) (this work), Au(111) [22], Au(100) [23], Ag(111) [24], and bilayer graphene on 6*H*-SiC(0001) [25]. On graphene and h-BN the electronic coupling of the first PTCDA ML to the respective substrate is rather weak, as evidenced by an absorption behavior reminiscent of dissolved molecules [34–36].

In contrast, on Au(111), Au(100), and Ag(111) the electronic coupling of the first ML to the substrate is much stronger. There, the stack structure is denoted as $PTCDA_{decoupled}$ on $PTCDA_{coupled}$/metal, and only the spectra of the second ML ($PTCDA_{decoupled}$) are analyzed using

$$\mathrm{DRS}^*(E,d^*) := \frac{R(E,d^*) - R(E,d_0)}{R(E,d_0)}. \qquad (2)$$

$R(E,d_0)$ denotes the reflectance of the modified substrate ($PTCDA_{coupled}$/metal), and the reduced nominal film thickness of $PTCDA_{decoupled}$ is $d^* = d - d_0$ with $d_0 = 1$ ML. Accordingly, the dielectric function of the physically second PTCDA ML ($d = 2$ ML), which is the first decoupled ML ($d^* = 1$ ML) on Au(111) [22], Au(100) [23], and Ag(111) [24] was extracted previously from DRS^* defined in Eq. (2).

In Ref. [7] optical spectroscopic ellipsometry revealed a Davydov splitting of $\Delta E_{\mathrm{Davydov}} = 37$ meV for the energetically lowest transition of α-PTCDA single crystals. Owing to similar molecular arrangements also for the β phase and PTCDA herringbone monolayer structures on various substrates, similar values for $\Delta E_{\mathrm{Davydov}}$ can be expected in all these cases. By contrast, the spectroscopic data discussed here were acquired with randomly polarized light and for samples which exhibit several rotational and/or mirror domains [33]. The two Davydov components can therefore not be probed independently. Instead, they contribute to the measured spectral broadening of the fundamental transition whose full width at half maximum (FWHM) is typically >100 meV at 300 K.

In all cases, except bilayer graphene on 6*H*-SiC(0001), the imaginary part ε'' of the dielectric function extracted from the DRS raw data was used for the spectral analysis [33,37]. For bilayer graphene on 6*H*-SiC(0001) the substrate's dielectric function is not known with sufficient accuracy [38,39], and thus the numerical algorithm used to extract the dielectric function of the adsorbate from the DRS raw data is not applicable [33,37]. The data can be analyzed nonetheless, because in the spectral region of interest graphene/SiC [38,39] is a transparent substrate and hence the DRS itself is proportional to ε'' in good approximation [40]. Since the dispersion of the optical constants of graphene/SiC is rather small in the spectral range of interest, the peak positions in DRS and ε'' spectra are almost identical.

The peak fitting procedure was carried out using the software ORIGINPRO 9.0.0G by OriginLab. For this purpose, the spectral range from 2.2 to 2.8 eV (in some cases up to 3.0 eV) was fitted by three (in some cases four) positive Gaussian peaks so as to satisfactorily reproduce the effective vibronic progression of the spectra while avoiding over-determination of the fit. As summarized in the Supplemental Material [41], we estimate the total uncertainty of the determined peak positions to be ± 10 meV for ≈ 0.2 ML and ± 8 meV for 1.0 ML of PTCDA on all the substrates discussed here. It is very important to realize that these conservative estimations for the maximum errors apply to specific single data points. The reproducibility of the determined $S_0 \rightarrow S_1$ transition energies in a given *series* of spectra is *much* better, since several sources of systematic errors are kept constant. For a given calibration of the spectrometer, choice of optical constants describing the substrate, and for unchanged constraints applied to the fitting model, the only truly statistical error sources are the drift of the DRS signal during the deposition and the standard deviation of the numerical peak fitting procedure. Drift during the optical data acquisition differs from experiment to experiment and can actually be orders of magnitude lower than the DRS

signal. This judgment is based on pre- and post-deposition drift measurements, yet the drift during the molecular deposition cannot be rigorously quantified due to our single-beam setup (no reference beam available).

For the specification of film thicknesses a constant molecular flux is assumed. This is reasonable owing to the actively controlled temperature of the crucible which was kept stable to within 1 K during deposition. Based on *in situ* DRS measurements several calibration marks are available for PTCDA deposited directly on Au(111) [22], Au(100) [23], and Ag(111) [24]: (1) The completion of the first coupled ML (wetting layer) is visible as an abrupt change from very broad to vibronically resolved spectra attributed to electronically decoupled second-layer molecules. (2) The completion of the first decoupled ML (physically second ML) is accompanied by a sudden change of the peak height ratio (which is rather constant between $d = 1$ and 2 ML), indicative of a monomer-dimer (or oligomer) transition of stacked molecules. (3) In the limit of thick films the dielectric functions extracted from DRS (or DRS*) converge toward the values independently determined for polycrystalline PTCDA on glass [42]. Importantly, the first two PTCDA MLs are known to grow in a layer-by-layer manner on Au(111) [43] and on Ag(111) [44]. Taking all these facts into account, a linear relationship between deposition time and amount of adsorbed molecules is revealed, which corroborates the above assumption of a constant molecular flux. The calibration marks (1) and (2) were reproducible within an uncertainty of ≈ 0.1 ML. STM images (not shown) of various samples were found to be consistent with this film thickness calibration. A similar procedure was carried out for graphene [25] and h-BN (this work), except that an electronically coupled PTCDA wetting layer is absent on these substrates.

In this manuscript we sometimes indicate film thicknesses used as a parameter for the extraction of the dielectric functions from the DRS (or DRS*) data with two decimal places. Thereby, we intend to minimize unnecessary rounding errors especially for submonolayer films whose thicknesses represent interpolated values. We emphasize that, according to the calibration procedures described above, the absolute film thicknesses are of course *not* known with an accuracy of 0.01 ML.

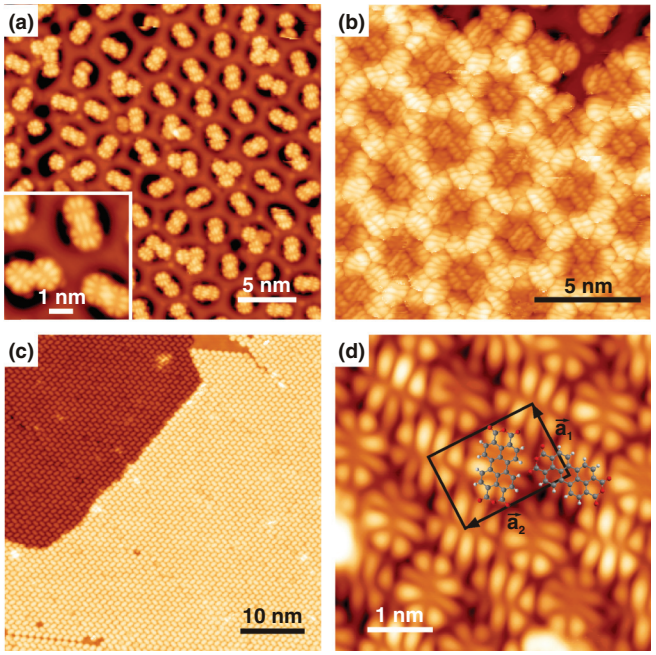

FIG. 1. STM images ($T_{STM} \approx 5$ K) of PTCDA deposits on metal-supported h-BN. All films were grown at $T_{substrate} = 300$ K. (a) Overview scan on h-BN/Rh(111) (−3.0 V, 200 pA) showing h-BN pores filled with molecules. (Inset) Close-up view on h-BN/Rh(111) with submolecular resolution of PTCDA (−3.0 V, 150 pA) depicting the orientation of the molecules in the pores. (b) Highly ordered, densely packed domain of PTCDA on h-BN/Rh(111) (−3.0 V, 300 pA) obtained after annealing at 400 K. (c) Overview scan on h-BN/Pt(111) (0.8 V, 100 pA) showing a highly ordered, densely packed PTCDA domain continuously grown across two substrate terraces. (d) Close-up view on h-BN/Pt(111) (−2.6 V, 200 pA) with submolecular resolution of PTCDA. A scheme of the two-molecule unit cell is superimposed.

III. RESULTS AND DISCUSSION

A. Structural characterization

Figure 1 summarizes the STM analysis of the growth of PTCDA on metal-supported monolayers of h-BN. The h-BN layers form distinct superstructures depending on the underlying metal substrate [45,46]. In the case of h-BN/Rh(111) a regular pattern of areas that are close to the substrate (pores) and intermediate regions (wires) is observed, where the PTCDA molecules adsorb preferentially in the pores of the h-BN layer, cf. Fig. 1(a). Further analysis of our experimental data revealed that the molecules try to follow the hexagonal symmetry of the h-BN lattice, leading to three preferential orientations of adsorption [inset of Fig. 1(a)] [47]. With increasing occupation of the pores with PTCDA molecules their preferential alignment cannot always be fulfilled due to the size restriction imposed by the pores. Additionally, each pore can act as a nucleus for domain formation, and the two-dimensional layer is characterized by tiny domains, a large number of packing defects, and many domain boundaries (not shown). Highly ordered, densely packed domains on h-BN/Rh(111) were only observed with subsequent annealing or elevated substrate temperature [above 370 K; Fig. 1(b)] during growth. This is likely caused by a higher lateral mobility of the molecules which enables some of them to diffuse beyond the pores and form larger aggregates. In contrast, the small corrugation of h-BN/Pt(111) allows for highly ordered, densely packed domains of PTCDA, achieved by room-temperature deposition. Subsequent annealing leads to extended domains with a small number of defects [Fig. 1(c)]. A fast Fourier transform of Fig. 1(c) yields the PTCDA lattice constants $|\vec{a}_1| = 1.281$ nm, $|\vec{a}_2| = 2.084$ nm, and $\Gamma = \sphericalangle(\vec{a}_1,\vec{a}_2) = 90.2°$ using the lattice parameters of h-BN/Pt(111) reported previously as calibration [32,48]. The ratio $|\vec{a}_2|/|\vec{a}_1| \approx 1.63$ is closer to α-PTCDA (≈ 1.66) than to β-PTCDA (≈ 1.55) [13–16]. The submolecular contrast of PTCDA on h-BN is dominated by the highest occupied molecular orbital (HOMO) of PTCDA [Figs. 1(a), 1(b), and 1(d)] [49].

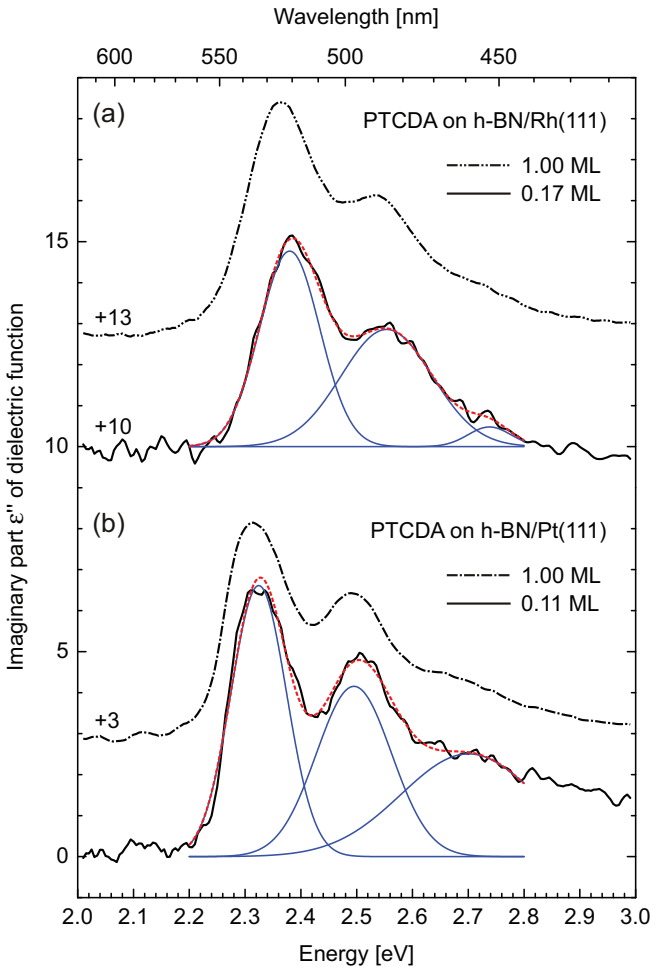

FIG. 2. Imaginary part ε'' of the dielectric function extracted from DRS measurements ($T = 300$ K) of PTCDA for selected coverages: (a) on h-BN/Rh(111) and (b) on h-BN/Pt(111). Peak fits using three Gaussian functions are exemplarily shown. Spectra are vertically offset for clarity.

B. Optical *in situ* DRS measurements

DRS measurements of PTCDA submonolayers and monolayers on h-BN/Rh(111) and on h-BN/Pt(111) were performed. Figure 2 depicts the extracted imaginary part ε'' of the dielectric function for selected nominal coverages. As opposed to PTCDA monolayers in direct contact with metal surfaces [22–24] the spectral shape on h-BN is almost not affected by the substrate, as evidenced by the vibronic progression resolved in Fig. 2. This means in turn that h-BN serves as a decoupling insulator, a behavior which has been reported before also for a hexa-*peri*-hexabenzocoronene monolayer on Au(111) and its effect on subsequently grown quaterrylene molecules [50].

The larger FWHM of the thin films on h-BN/Rh(111) as compared with those on h-BN/Pt(111) may be attributed to an increased inhomogeneous line broadening owing to the inferior degree of order on the former substrate. Such a comparison of FWHMs is possible in this case, because both metal substrates are covered by an h-BN monolayer and are thus chemically rather equivalent. However, a comparison with FWHMs measured for PTCDA on other substrates is complicated due to chemically different surface terminations. Although the molecule-substrate interaction is weak in all the cases discussed in this contribution, slight differences cannot be ruled out. Consequently, we refrain from comparing FWHMs on all substrates used in this study.

C. Analysis of the optical $S_0 \rightarrow S_1$ transition

1. *Dissolved PTCDA*

PTCDA is poorly soluble in many solvents, especially in nonpolar media. Therefore, only the room-temperature spectra of PTCDA in chloroform ($CHCl_3$) [35], dichloromethane (CH_2Cl_2) [36], and dimethyl sulfoxide (DMSO) [34] were analyzed here; cf. Fig. 3. A reliable expectation for the transition energy in a nonpolar solvent cannot be simply extracted from these data because (i) only few data points are available, (ii) it is not known how the solvation precisely takes place, i.e., how the permanent dipoles of the solvent molecules align microscopically with the PTCDA chromophores, and (iii) apart from the dissimilar polar nature of these solvents also the different dielectric constants (polarizabilities) influence the measured spectral positions.

At $T = 0.38$ K the purely electronic component of the $S_0 \rightarrow S_1$ transition (i.e., the fundamental transition) was

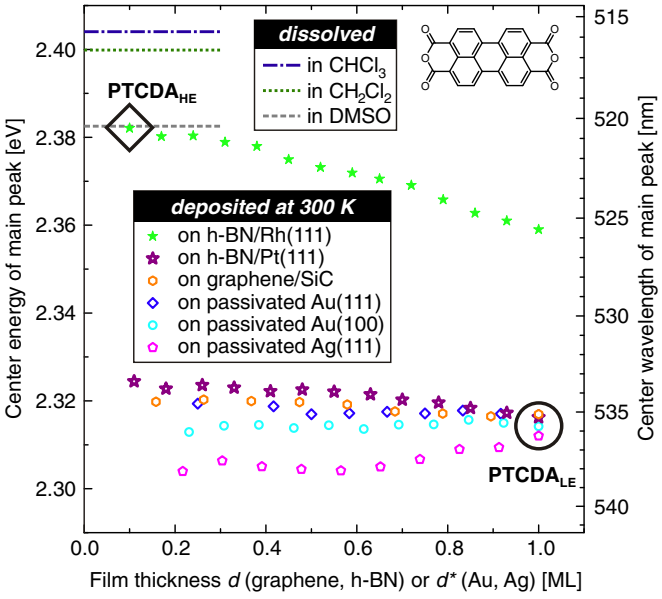

FIG. 3. Comparison of the center energy of the $S_0 \rightarrow S_1$ fundamental transition of PTCDA on various substrates. On graphene and h-BN the electronic coupling of the first ML to the substrate is weak, so that the spectra are reminiscent of PTCDA in solution. On Au(111) [22], Au(100) [23], and Ag(111) [24] the electronic coupling of the first ML to the substrate is strong. There, the spectra of the second ML were analyzed, and accordingly, the reduced film thickness d^* on the passivated coinage metals is given; cf. Eq. (2). The transition energies of PTCDA dissolved in $CHCl_3$, CH_2Cl_2, and DMSO are also indicated [34–36]. The data points highlighted by the black diamond and the black circle are those closest to the ideal case of isolated monomers and two-dimensional herringbone aggregates, respectively; see the text for details.

obtained for PTCDA in helium nanodroplets at 2.6022 eV (20 988 cm^{-1}) with laser-induced fluorescence (LIF) spectroscopy [51]. In principle, this value should closely mimic the transition energy for gas-phase PTCDA, i.e., molecules in the limit of vanishing temperature and in an interaction-free environment with negligible dielectric polarizability. For PTCDA attached to solid clusters of Ne at $\approx$ 10 K and Ar at $\approx$ 35 K the fundamental transition was also measured with LIF spectroscopy at 2.5786 eV (20 798 cm^{-1}) and 2.5061 eV (20213 cm^{-1}), respectively, though somewhat broadened as compared to the data in He [52]. Although the spectral shifts ΔE scale with the static polarizabilities α of the rare gases, the observed relation $\Delta E(\alpha)$ falls below a linear dependence notably for higher values of α [52].

It has been demonstrated previously that photoluminescence (PL) spectra of other conjugated molecules, such as *para*-hexaphenyl, exhibit a sizable red-shift (several tens of meV) when the sample temperature is raised from 30 to 290 K which was explained by interactions between the electrons and molecular vibrations or librations [53,54]. Since this red-shift was also reported to depend on the conjugation of the chromophore [53], an even stronger temperature effect might be present for PTCDA; hence the comparison of absolute peak positions recorded at different temperatures is not readily feasible.

2. PTCDA monolayers on various substrates

In Fig. 3 we present the results of the peak fit analysis performed on the optical $S_0 \rightarrow S_1$ transition of PTCDA on various substrates. The spectral positions of PTCDA on h-BN/Pt(111) and graphene/SiC(0001) (first-layer molecules) as well as on Au(111), Au(100), and Ag(111) (second-layer molecules) are all identical to within $\pm$10 meV and almost coverage independent between 0 and 1 ML. At 1 ML the spectral positions of PTCDA on these substrates can hardly be distinguished within the experimental accuracy, as highlighted in Fig. 3 by a black circle. In contrast, all the main peak positions of PTCDA films on h-BN/Rh(111) are evidently located at noticeably higher energies, and they exhibit a distinct tendency towards lower energies upon coverage increase.

3. Interpretation

One possible reason for different spectral positions could be the dissimilar polarizabilities of the substrates [38,39,55,56]. However, this cannot be the dominant effect here since the spectral positions of PTCDA grown on top of all substrates except h-BN/Rh(111) are almost identical, which is especially true for the spectra of 1 ML PTCDA. In fact, the possible influence of dissimilar polarizabilities can be readily assessed: In a simple explanatory approach, an oscillating electric dipole above a metal surface can be treated classically. An electric dipole virtually creates an image dipole within the metal. The interaction energy J_{mn} between two optical transition dipoles can be estimated using the formula for pointlike dipoles [57]:

$$J_{mn} = \frac{1}{4\pi\varepsilon_0} \cdot \left[\frac{\vec{\mu}_m \cdot \vec{\mu}_n}{r^3} - 3 \cdot \frac{(\vec{\mu}_m \cdot \vec{r}) \cdot (\vec{\mu}_n \cdot \vec{r})}{r^5} \right], \qquad (3)$$

where $\vec{r}$ is the vector pointing from transition dipole $\vec{\mu}_m$ to $\vec{\mu}_n$ (with $r = |\vec{r}|$). For horizontally adsorbed PTCDA whose $S_0 \rightarrow S_1$ transition dipole lies within the molecular plane (i.e., parallel to the interface), this simplifies to

$$J_{mn} = -\frac{1}{4\pi\varepsilon_0 r^3} \cdot |\vec{\mu}_m| \cdot |\vec{\mu}_n|, \qquad (4)$$

because in this case we have $(\vec{\mu}_m \cdot \vec{r}) = (\vec{\mu}_n \cdot \vec{r}) = 0$ and $\vec{\mu}_m \cdot \vec{\mu}_n = |\vec{\mu}_m| \cdot |\vec{\mu}_n| \cdot \cos 180^\circ = -|\vec{\mu}_m| \cdot |\vec{\mu}_n|$. This means that a horizontal transition dipole moment $\vec{\mu}_{||}$ experiences an interaction with the metal surface that causes a red-shift which depends sensitively on the distance from the interface. For metals, characterized by the complex dielectric function $\varepsilon_{\text{metal}}(\omega)$, Eq. (4) reads

$$J_{mn} = -\frac{1}{4\pi\varepsilon_0 r^3} \cdot |\vec{\mu}_{||}|^2 \cdot \text{Re}\left(\frac{\varepsilon_{\text{metal}}(\omega) - 1}{\varepsilon_{\text{metal}}(\omega) + 1} \right). \qquad (5)$$

A similar expression has been derived in the framework of quantum electrodynamics for a harmonic oscillator [60,61]. Note that the distance to be used in Eq. (5) is twice the adsorption height above the metal, i.e., $r = 2h$. Here, we focus on PTCDA that is decoupled from the metal by a monolayer of either h-BN or $\text{PTCDA}_{\text{coupled}}$, hence h is in the order of 0.64 nm. Table I summarizes the expected shifts J_{mn} of the $S_0 \rightarrow S_1$ transition energies. Note that the dielectric screening caused by the polarizability either of the h-BN monolayer (on Rh, Pt) or of the first PTCDA layer (on Au, Ag) is neglected in this simple estimation, as it is not readily quantifiable. However, this should not affect the red-shift substantially. We conclude that polarizability effects of the metal surfaces are indeed expected to cause spectral shifts which differ only slightly between the different substrates used. Yet, they do by far not account for the difference of approximately 70 meV between PTCDA_{HE} [on h-BN/Rh(111)] and PTCDA_{LE} [e.g., on h-BN/Pt(111)]. This estimation demonstrates that the polarizabilities of the metal substrates do not constitute the dominant contribution to the molecular $S_0 \rightarrow S_1$ transition energies observed here.

Also, different molecular conformers are unlikely to account for the observed spectral positions. Molecule-substrate interactions, which might cause bending or twisting of the chromophores, can be classified as covalent (i.e., hybridization, charge transfer) or noncovalent (i.e., Coulomb interaction, van der Waals attraction, Pauli repulsion). For the molecular layers discussed here, covalent and Coulomb interactions with the respective substrates should be negligible. The flat molecular geometry of PTCDA is presumably not altered when adsorbed on the inert h-BN and graphene surfaces. Similarly, several studies report an essentially unaltered

TABLE I. Expected shifts J_{mn} of the $S_0 \rightarrow S_1$ transition energies using Eq. (5) at the photon wavelength $\lambda = 536$ nm ($\hbar\omega = 2.313$ eV) using $|\vec{\mu}_{||}| = 7.4$ D for PTCDA from Ref. [58].

	Ag	Au	Pt	Rh
Data source	Ref. [56]	Ref. [56]	Ref. [55]	Ref. [59]
$\text{Re}(\varepsilon_{\text{metal}}(\omega))$	−11.942	−4.691	−9.015	−20.444
$\text{Im}(\varepsilon_{\text{metal}}(\omega))$	0.358	1.549	14.891	19.027
$\text{Re}\left(\frac{\varepsilon_{\text{metal}}(\omega)-1}{\varepsilon_{\text{metal}}(\omega)+1}\right)$	1.183	1.461	1.056	1.053
J_{mn} (meV)	−19	−24	−17	−17

geometry of first-layer PTCDA on Au(111) [62,63] which renders a deformation of second-layer molecules (analyzed here) unlikely. As opposed to the weakly interacting substrates above it is known that the geometry of chemisorbed first-layer PTCDA is modified on Ag(111) [62,63]; yet, we do not expect this to be significant for second-layer molecules due to the much weaker interaction between the first and second ML of PTCDA than with Ag(111).

Aggregation effects therefore remain to be discussed. In fact, the film structures of PTCDA monolayers (and in some cases also multilayers) on Au(111) [64,65], Au(100) [64], Ag(111) [44], and graphene or graphite [25,66] are well known. Additionally, the film structure of PTCDA on h-BN/Pt(111) is elucidated in Figs. 1(c) and 1(d). In essence, PTCDA forms highly ordered layers consisting of densely packed, extended domains on *all* these substrates. By contrast, PTCDA adsorbs first in the pores of h-BN/Rh(111) [cf. Fig. 1(a)], which all act as aggregation centers of small domains. Highly ordered domains could only be achieved by annealing; cf. Fig. 1(b). This means in turn that the lateral aggregation differs noticeably for h-BN/Rh(111) as compared to the other substrates and may explain the spectral differences.

Consequently, we have to distinguish between two physical molecular species, $\mathrm{PTCDA_{LE}}$ and $\mathrm{PTCDA_{HE}}$, according to the prevailing $S_0 \rightarrow S_1$ transition energy.

$\mathrm{PTCDA_{LE}}$ spectra are attributed to highly ordered, densely packed 2D herringbone domains. We assume that these domains have already formed at 0.2 ML or below owing to a high lateral mobility at 300 K. At this point they have reached a sufficient size, so that lateral extension upon coverage increase to 1 ML barely influences the spectral position further, as deduced from the nearly absent thickness dependence of the $\mathrm{PTCDA_{LE}}$ transition energy. The critical domain size to account for most of this spectral difference (with respect to $\mathrm{PTCDA_{HE}}$) is probably quite small, given that the characteristic distance of exciton delocalization in the (102) plane of a PTCDA bulk crystal is much less pronounced than in the stacking direction [17]. Nevertheless, we note that quite large arrays of $\approx 400 \times 400$ unit cells were necessary to reach convergence in excitonic band structure calculations using a tight-binding approach [26].

By comparison with solution spectra, $\mathrm{PTCDA_{HE}}$ comes energetically closer to the ideal case of "isolated monomers" (i.e., influences from the molecular environment are negligible) than $\mathrm{PTCDA_{LE}}$ does. $\mathrm{PTCDA_{HE}}$ spectra are thus attributed to scattered molecules on the surface. This means that either the molecules are subject to repulsive lateral interaction or that the surface morphology significantly hampers the diffusion of the molecules and thus the growth of domains. The former scenario is atypical for PTCDA which has a strong tendency to form extended close-packed domains on many substrates at 300 K [67]. The latter situation is likely encountered on h-BN/Rh(111) which looks like a muffin tin [Fig. 1(a)]. Interestingly, the fundamental transition energy of very dilute PTCDA deposits (less than 1% of a monolayer equivalent) on a tapered glass fiber was found previously at 2.40–2.42 eV [68], which is close to the $\mathrm{PTCDA_{HE}}$ peak position observed here.

The two limiting cases are highlighted in Fig. 3: The center energy of the main peak is roughly 2.38 eV for isolated monomers ($\mathrm{PTCDA_{HE}}$ at low coverage) and about 2.31 eV for the herringbone domains ($\mathrm{PTCDA_{LE}}$ at 1 ML), meaning that a red-shift of $\Delta E_{\mathrm{HE\text{-}LE}} \approx 70$ meV is caused by this 2D domain formation.

4. Comparison with PTCDA on NaCl(100) and KCl(100)

A red-shift of PL and photoluminescence excitation (PLE) spectra from a dilute phase (<0.01 ML) to a herringbone monolayer phase ["HB* phase," similar to the (102) plane of β-PTCDA] by $\Delta E_{\mathrm{dilute\text{-}HB^*}} = 69.4$ meV (560 $\mathrm{cm^{-1}}$) was also observed for PTCDA on NaCl(100) [26]. This is in remarkable accordance with the red-shift $\Delta E_{\mathrm{HE\text{-}LE}}$ observed here and further corroborates the above interpretation. The authors of Ref. [26] assessed the excitonic band structures of 2D PTCDA aggregates using a tight-binding approach. At the Γ point of the Brillouin zone the dispersion branch of the HB* phase was calculated to be $\Delta E_{\Gamma} = 28.5$ meV (230 $\mathrm{cm^{-1}}$) lower than for the dispersion-free case, i.e., isolated monomers. The remaining difference between the computed excitonic band structure and the experiment was attributed by them to polarization effects within the condensed HB* phase, i.e., $\Delta E_{\mathrm{pol}} = \Delta E_{\mathrm{dilute\text{-}HB^*}} - \Delta E_{\Gamma} = 40.9$ meV (330 $\mathrm{cm^{-1}}$).

Please note that the absolute energies can differ significantly even for similar optical techniques. For instance, the 0-0 transition of the "brickwall" monolayer phase on 10 ML KCl(100)/Ag(100) [69,70] was found at ≈ 2.480 eV ($(20\,000 \pm 20)$ $\mathrm{cm^{-1}}$) with PLE (PTCDA deposited at 260 K, measured at 20 K), while on bulk KCl(100) [71] it was measured at 2.431 eV with DRS at 300 K during deposition. This comparison shows that even on the same substrate (10 ML KCl can be considered bulklike) and for the same molecular monolayer structure the fundamental transition is found at different energies, ≈ 50 meV (≈ 400 $\mathrm{cm^{-1}}$) apart. This discrepancy compares favorably with that observed for *para*-hexaphenyl with PL spectroscopy at different temperatures as mentioned above [53]. Therefore, only the peak shifts are discussed here.

Müller *et al.* compared their PL data for the dilute phase on NaCl(100) [26] to the measurements by Wewer and Stienkemeier recorded in helium nanodroplets [51] so as to estimate the gas-to-surface shift $\Delta E_{\mathrm{gas\text{-}dilute}}$ of single molecules. They found that in both cases, apart from the rigid shift $\Delta E_{\mathrm{gas\text{-}dilute}} = 162$ meV (1307 $\mathrm{cm^{-1}}$), the spectral positions and relative intensities are rather similar for the modes observed in the spectral region from $\approx 17\,300$ $\mathrm{cm^{-1}}$ to 20 000 $\mathrm{cm^{-1}}$. Based on the data available at that time, the authors concluded that the molecular geometry of PTCDA was not significantly altered upon adsorption on the NaCl(100) surface. Consequently, they attributed $\Delta E_{\mathrm{gas\text{-}dilute}}$ solely to the polarization of the alkali-metal halide substrate assuming a vanishing polarizability of He (identical to vacuum). However, recent DFT calculations came to a different conclusion, namely that PTCDA is bent markedly due to the bonding with the NaCl(100) surface [72–74]. The authors of Ref. [74] computed the absorption energies for the gas-phase molecule and for an isolated molecule on the alkali-metal halide surface which, according to them, differ by 114 meV (for the 6-311G* basis set), of which $\Delta E_{\mathrm{dist}} = 26$ meV are caused by molecular distortion and $\Delta E_{\mathrm{elec}} = 36$ meV by electrostatic interaction

between PTCDA and NaCl. While these numbers depend on the employed basis set, they demonstrate nonetheless that more factors contribute significantly to the measured shift $\Delta E_{\text{gas-dilute}}$ than merely the substrate polarizability. The effect of the latter is in fact sometimes overestimated.

Unfortunately, such calculations of the transition energies are not available for a PTCDA ML on NaCl(100). If one assumes that the distortion of the molecules, the covalent as well as the noncovalent [75] interactions between molecules and substrate, and the polarizability of the substrate do not differ substantially for the HB* phase as compared to the dilute phase, then $\Delta E_{\text{dilute-HB}^*}$ can be mainly ascribed to the formation of excitonic bands and to the polarizability of the molecular environment [26]. For similar reasons we also attribute $\Delta E_{\text{HE-LE}}$ primarily to these 2D domain formation effects of PTCDA which is the most notable discrepancy between h-BN/Rh(111) and the other substrates discussed here.

5. Domain formation on metal-supported h-BN

Further information can be gathered from a more detailed comparison of the data on h-BN/Rh(111) and on h-BN/Pt(111). The PTCDA domain size is limited by the surface morphology of the h-BN layer which is very different on both metal substrates [31,32]. Given that we observe sizeable PTCDA domains on h-BN/Pt(111) even at submonolayer coverage but only tiny PTCDA islands on h-BN/Rh(111), the different domain formation behavior on both substrates should cause dissimilar red-shifts. Indeed, the $S_0 \rightarrow S_1$ transition shifts by only $-(8.8 \pm 0.8)$ meV/ML on h-BN/Pt(111), while the shift on h-BN/Rh(111) amounts to $-(27.6 \pm 0.7)$ meV/ML, as determined from linear fits to the data in Fig. 3 [76]. We do not intend to put too much emphasis on these absolute values, but it is evident that the latter slope is clearly more significant than the former.

Interestingly, our structural characterization of PTCDA on h-BN/Rh(111) revealed that the molecules adsorb in the pores first, and only when they are filled the molecules also adsorb on the wires surrounding the pores. The depth of the pores is about 0.7 Å [31], thus the molecules adsorbing on the wires are significantly further away from the metal surface than those in the pores. In the view of the estimated spectral shift attributed to the coupling to an image dipole within the metal, see Eq. (5), this leads to the expectation that the $S_0 \rightarrow S_1$ transition should shift to higher energies (by several meV) with increasing coverage on h-BN/Rh(111) and hence increasing average distance of the molecules from the metal surface. Quite clearly, we observe the opposite trend with a significant red-shift upon coverage increase. Again, this leads us to the conclusion that the substrate's polarizability is not the dominant contribution for the observed peak positions and that it is outweighed by the effect of two-dimensional aggregation, i.e., molecular domain formation. We note that the almost coverage-independent $S_0 \rightarrow S_1$ transition energy of PTCDA on h-BN/Pt(111) is explainable by highly ordered domains which, in accordance with our structural characterization of that system, have reached a sufficient average size to account for the PTCDA_{LE} spectral position already at submonolayer coverage.

6. Molecular migration of PTCDA_{HE} films

Here, we briefly comment on structural rearrangements of as-deposited films which may occur as a function of time. On flat h-BN the lateral mobility at 300 K is sufficiently high for individual molecules to migrate almost freely and for the film structure to achieve a dynamic equilibrium much faster than the integration intervals of the DRS measurements. For h-BN/Rh(111) in particular, the adsorption energy gain within the pores is markedly higher than on the wires, so that the molecules become trapped inside the pores. For phthalocyanine molecules, this has been investigated in detail in Ref. [77]. We could not determine a significant tendency of the individual PTCDA molecules in the pores to migrate and to form domains when the substrate was kept at 300 K. Consequently, although molecular migration is a known effect described in the literature [78–80], it cannot be traced in the room-temperature optical measurements of as-deposited PTCDA films on h-BN/Rh(111). At elevated temperatures (above roughly 400 K) the latter do indeed rearrange and form extended domains. However, heating the substrates from 300 to 400 K during DRS experiments causes significant thermal drift (instabilities of the sample manipulator and hence of the reflection geometry) which would render a spectral analysis difficult.

IV. SUMMARY AND CONCLUSION

In summary, of all examples considered in this work the optical absorption spectra of PTCDA on h-BN/Rh(111), especially at low coverage, come closest to the ideal case of isolated monomers. In contrast, the spectra of PTCDA on all other substrates discussed here, particularly at monolayer coverage, are attributed to two-dimensional aggregates composed of densely packed, highly ordered herringbone domains with flat-lying molecules, similar to the (102) planes of PTCDA bulk crystals. The center energy of the fundamental transition measured at 300 K is approximately 2.38 eV (HE component) for isolated monomers and about 2.31 eV (LE component) for the herringbone monolayers, meaning that a red-shift of ≈ 70 meV is caused by the formation of extended 2D domains. This compares favorably with previous measurements of PTCDA on NaCl(100) [26] where the red-shift from a dilute phase to a herringbone monolayer phase was determined as 69.4 meV. This remarkable accordance suggests that the same physical effects are responsible for the red-shift. Two contributions have been identified in the literature [26]: (i) the polarizability of neighboring molecules, and (ii) the formation of excitonic bands, both being characteristic for densely packed monolayers.

Other possible effects, such as different molecular geometries or dissimilar dielectric properties of the substrates, are hardly eligible to account for the systematic observation of PTCDA_{HE} and PTCDA_{LE} species. One key argument here is the occurrence of PTCDA_{HE} on h-BN/Rh(111) and of PTCDA_{LE} on h-BN/Pt(111), i.e., two metal substrates covered by a passivating h-BN layer unlikely to cause significant molecular deformations or electronic coupling with PTCDA. Further, PTCDA_{LE} is also observed at almost the same transition energy on graphene/SiC and for the second molecular layer on noble metals, i.e., on various substrates with decisively different dielectric functions.

We conclude that the $S_0 \rightarrow S_1$ transition energy of PTCDA is markedly influenced by the 2D aggregation behavior which itself depends on the templating effect imposed by the substrate. Notably, the spectral envelope is hardly affected by the 2D PTCDA herringbone structure as compared to solution spectra. This is different from the so-called brickwall structure on KCl(100) where all chromophores are aligned parallel and form J aggregates.

ACKNOWLEDGMENTS

R.F., M.G., M.M., T.K., and T.F. thank the Deutsche Forschungsgemeinschaft for funding through Grants No. FR 875/9-3 and No. FO 770/2-1. T.K. further acknowledges financial support from the Evonik Stiftung. T.D. and O.G. would like to thank the Swiss National Science Foundation for financial support (Grant No. SNF-200021_149627).

[1] S. Reineke, M. Thomschke, B. Lüssem, and K. Leo, Rev. Mod. Phys. **85**, 1245 (2013).
[2] K. Walzer, B. Maennig, M. Pfeiffer, and K. Leo, Chem. Rev. **107**, 1233 (2007).
[3] A. Mishra and P. Bäuerle, Angew. Chem. Int. Ed. **51**, 2020 (2012).
[4] M. Pope and C. E. Swenberg, *Electronic Processes in Organic Crystals and Polymers*, 2nd ed. (Oxford University Press, New York, 1999).
[5] M. Kozlik, S. Paulke, M. Gruenewald, R. Forker, and T. Fritz, Org. Electron. **13**, 3291 (2012).
[6] K. Wihksne and A. E. Newkirk, J. Chem. Phys. **34**, 2184 (1961).
[7] M. I. Alonso, M. Garriga, N. Karl, J. O. Ossó, and F. Schreiber, Org. Electron. **3**, 23 (2002).
[8] N. Karl, Synth. Met. **133-134**, 649 (2003).
[9] N. Ueno and S. Kera, Prog. Surf. Sci. **83**, 490 (2008).
[10] F. Ortmann, F. Bechstedt, and K. Hannewald, Phys. Status Solidi B **248**, 511 (2011).
[11] C. Schünemann, D. Wynands, K.-J. Eichhorn, M. Stamm, K. Leo, and M. Riede, J. Phys. Chem. C **117**, 11600 (2013).
[12] F. Quochi, G. Schwabegger, C. Simbrunner, F. Floris, M. Saba, A. Mura, H. Sitter, and G. Bongiovanni, Adv. Optical Mater. **1**, 117 (2013).
[13] T. Ogawa, K. Kuwamoto, S. Isoda, T. Kobayashi, and N. Karl, Acta Crystallogr., Sect. B **55**, 123 (1999).
[14] K. Tojo and J. Mizuguchi, Z. Kristallogr.–New Cryst. Struct. **217**, 253 (2002).
[15] K. Tojo and J. Mizuguchi, Z. Kristallogr.–New Cryst. Struct. **217**, 255 (2002).
[16] A. A. Levin, T. Leisegang, R. Forker, M. Koch, D. C. Meyer, and T. Fritz, Cryst. Res. Technol. **45**, 439 (2010).
[17] S. Sharifzadeh, A. Biller, L. Kronik, and J. B. Neaton, Phys. Rev. B **85**, 125307 (2012).
[18] M. Hoffmann and Z. G. Soos, Phys. Rev. B **66**, 024305 (2002).
[19] M. Hoffmann, in *Electronic Excitations in Organic Multilayers and Organic Based Heterostructures*, Thin Films and Nanostructures, Vol. 31, edited by V. M. Agranovich and G. F. Bassani (Elsevier, Amsterdam, 2003), Chap. 5, p. 221.
[20] H. Proehl, T. Dienel, R. Nitsche, and T. Fritz, Phys. Rev. Lett. **93**, 097403 (2004).
[21] H. Proehl, R. Nitsche, T. Dienel, K. Leo, and T. Fritz, Phys. Rev. B **71**, 165207 (2005).
[22] R. Forker, C. Golnik, G. Pizzi, T. Dienel, and T. Fritz, Org. Electron. **10**, 1448 (2009).
[23] R. Forker, *Electronic Coupling Effects and Charge Transfer between Organic Molecules and Metal Surfaces*, Dissertation, Technische Universität, Dresden, 2010.
[24] M. Gruenewald, K. Wachter, M. Meissner, M. Kozlik, R. Forker, and T. Fritz, Org. Electron. **14**, 2177 (2013).
[25] M. Meissner, M. Gruenewald, F. Sojka, C. Udhardt, R. Forker, and T. Fritz, Surf. Sci. **606**, 1709 (2012).
[26] M. Müller, E. Le Moal, R. Scholz, and M. Sokolowski, Phys. Rev. B **83**, 241203(R) (2011).
[27] M. T. Paffett, R. J. Simonson, P. Papin, and R. T. Paine, Surf. Sci. **232**, 286 (1990).
[28] M. Corso, W. Auwärter, M. Muntwiler, A. Tamai, T. Greber, and J. Osterwalder, Science **303**, 217 (2004).
[29] S. Berner, M. Corso, R. Widmer, O. Groening, R. Laskowski, P. Blaha, K. Schwarz, A. Goriachko, H. Over, S. Gsell, M. Schreck, H. Sachdev, T. Greber, and J. Osterwalder, Angew. Chem. Int. Ed. **46**, 5115 (2007).
[30] R. Widmer, D. Passerone, T. Mattle, H. Sachdev, and O. Gröning, Nanoscale **2**, 502 (2010).
[31] T. Greber, M. Corso, and J. Osterwalder, Surf. Sci. **603**, 1373 (2009).
[32] E. Ćavar, R. Westerström, A. Mikkelsen, E. Lundgren, A. S. Vinogradov, M. L. Ng, A. B. Preobrajenski, A. A. Zakharov, and N. Mårtensson, Surf. Sci. **602**, 1722 (2008).
[33] R. Forker, M. Gruenewald, and T. Fritz, Annu. Rep. Prog. Chem., Sect. C: Phys. Chem. **108**, 34 (2012).
[34] V. Bulović, P. E. Burrows, S. R. Forrest, J. A. Cronin, and M. E. Thompson, Chem. Phys. **210**, 1 (1996).
[35] K. Gustav, M. Leonhardt, and H. Port, Monatsh. Chem. **128**, 105 (1997).
[36] U. Gómez, M. Leonhardt, H. Port, and H. C. Wolf, Chem. Phys. Lett. **268**, 1 (1997).
[37] R. Nitsche and T. Fritz, Phys. Rev. B **70**, 195432 (2004).
[38] S. Singh, J. R. Potopowicz, L. G. Van Uitert, and S. H. Wemple, Appl. Phys. Lett. **19**, 53 (1971).
[39] J. Chen, Z. H. Levine, and J. W. Wilkins, Phys. Rev. B **50**, 11514 (1994).
[40] J. D. E. McIntyre and D. E. Aspnes, Surf. Sci. **24**, 417 (1971).
[41] See Supplemental Material at http://link.aps.org/supplemental/10.1103/PhysRevB.93.165426 for a detailed account of the various sources of experimental error.
[42] A. B. Djurišić, T. Fritz, and K. Leo, Opt. Commun. **183**, 123 (2000).
[43] I. Chizhov, A. Kahn, and G. Scoles, J. Cryst. Growth **208**, 449 (2000).
[44] L. Kilian, E. Umbach, and M. Sokolowski, Surf. Sci. **573**, 359 (2004).
[45] R. Laskowski and P. Blaha, Phys. Rev. B **81**, 075418 (2010).
[46] J. Gómez Díaz, Y. Ding, R. Koitz, A. P. Seitsonen, M. Iannuzzi, and J. Hutter, Theor. Chem. Acc. **132**, 1350 (2013).
[47] T. Dienel, J. Gómez-Díaz, A. P. Seitsonen, R. Widmer, M. Iannuzzi, K. Radican, H. Sachdev, K. Müllen, J. Hutter, and O. Gröning, ACS Nano **8**, 6571 (2014).

[48] S. M. Foiles, M. I. Baskes, and M. S. Daw, Phys. Rev. B **33**, 7983 (1986).
[49] A. J. Martínez-Galera, N. Nicoara, J. I. Martínez, Y. J. Dappe, J. Ortega, and J. M. Gómez-Rodríguez, J. Phys. Chem. C **118**, 12782 (2014).
[50] R. Forker, D. Kasemann, T. Dienel, C. Wagner, R. Franke, K. Müllen, and T. Fritz, Adv. Mater. **20**, 4450 (2008).
[51] M. Wewer and F. Stienkemeier, J. Chem. Phys. **120**, 1239 (2004).
[52] M. Dvorak, M. Müller, T. Knoblauch, O. Bünermann, A. Rydlo, S. Minniberger, W. Harbich, and F. Stienkemeier, J. Chem. Phys. **137**, 164301 (2012).
[53] S. Guha, J. D. Rice, Y. T. Yau, C. M. Martin, M. Chandrasekhar, H. R. Chandrasekhar, R. Guentner, P. Scanduicci de Freitas, and U. Scherf, Phys. Rev. B **67**, 125204 (2003).
[54] T. Basché, W. E. Moerner, M. Orrit, and U. P. Wild (eds.), *Single-Molecule Optical Detection, Imaging and Spectroscopy* (VCH, Weinheim, 1997).
[55] A. D. Rakić, A. B. Djurišić, J. M. Elazar, and M. L. Majewski, Appl. Opt. **37**, 5271 (1998).
[56] S. Babar and J. H. Weaver, Appl. Opt. **54**, 477 (2015).
[57] M. Kasha, H. R. Rawls, and M. A. El-Bayoumi, Pure Appl. Chem. **11**, 371 (1965).
[58] M. Hoffmann, K. Schmidt, T. Fritz, T. Hasche, V. M. Agranovich, and K. Leo, Chem. Phys. **258**, 73 (2000).
[59] J. H. Weaver, C. G. Olson, and D. W. Lynch, Phys. Rev. B **15**, 4115 (1977).
[60] J. M. Wylie and J. E. Sipe, Phys. Rev. A **32**, 2030 (1985).
[61] M. Fichet, F. Schuller, D. Bloch, and M. Ducloy, Phys. Rev. A **51**, 1553 (1995).
[62] S. K. M. Henze, O. Bauer, T.-L. Lee, M. Sokolowski, and F. S. Tautz, Surf. Sci. **601**, 1566 (2007).
[63] V. G. Ruiz, W. Liu, E. Zojer, M. Scheffler, and A. Tkatchenko, Phys. Rev. Lett. **108**, 146103 (2012).
[64] S. Mannsfeld, M. Toerker, T. Schmitz-Hübsch, F. Sellam, T. Fritz, and K. Leo, Org. Electron. **2**, 121 (2001).
[65] L. Kilian, E. Umbach, and M. Sokolowski, Surf. Sci. **600**, 2633 (2006).
[66] A. Hoshino, S. Isoda, H. Kurata, and T. Kobayashi, J. Appl. Phys. **76**, 4113 (1994).
[67] F. S. Tautz, Prog. Surf. Sci. **82**, 479 (2007).
[68] F. Warken, E. Vetsch, D. Meschede, M. Sokolowski, and A. Rauschenbeutel, Opt. Express **15**, 11952 (2007).
[69] M. Müller, J. Ikonomov, and M. Sokolowski, Surf. Sci. **605**, 1090 (2011).
[70] M. Müller, A. Paulheim, A. Eisfeld, and M. Sokolowski, J. Chem. Phys. **139**, 044302 (2013).
[71] T. Dienel, C. Loppacher, S. C. B. Mannsfeld, R. Forker, and T. Fritz, Adv. Mater. **20**, 959 (2008).
[72] H. Aldahhak, W. G. Schmidt, and E. Rauls, Surf. Sci. **617**, 242 (2013).
[73] H. Aldahhak, W. G. Schmidt, and E. Rauls, Surf. Sci. **641**, 278 (2015).
[74] M. Hochheim and T. Bredow, J. Comput. Chem. **36**, 1805 (2015).
[75] C. Sutton, C. Risko, and J.-L. Brédas, Chem. Mater. **28**, 3 (2016).
[76] For this purpose, the systematic errors are not taken into account, since they influence each data point in a similar way and are thus insignificant for the determination of slopes within a series of spectral positions.
[77] M. Iannuzzi, F. Tran, R. Widmer, T. Dienel, K. Radican, Y. Ding, J. Hutter, and O. Gröning, Phys. Chem. Chem. Phys. **16**, 12374 (2014).
[78] S. Kera, K. K. Okudaira, Y. Harada, and N. Ueno, Jpn. J. Appl. Phys. **40**, 783 (2001).
[79] D. G. de Oteyza, E. Barrena, S. Sellner, J. O. Ossó, and H. Dosch, J. Phys. Chem. B **110**, 16618 (2006).
[80] T. Sugiyama, T. Sasaki, S. Kera, N. Ueno, and T. Munakata, Chem. Phys. Lett. **449**, 319 (2007).